REPORT ON LIGO INTERFEROMETERS

I. Initial Design and Performance for Three Sample Configurations

Alex Abramovici Peter Saulson Robert Spero

18 April 1989

Abstract

Elements of the conceptual design relating to ligo interferometers are collected, analyzed, and combined into three model systems spanning a wide range of sensitivity; evaluation of performance as limited by dominant noise sources is presented.

1 Credits and Caveats

The present state of ligo interferometer design is the result of several years of evolution of concepts, driven strongly by experimental work. This report draws heavily on *Outline of a Proposed Design for a First Receiver for Installation in the Long-Baseline Facilities, of Fabry-Perot Type (September 10, 1987)*, by R. Drever, and on several technical studies recently completed by the science teams. Nonetheless, some parts of the design and analysis we present have come to light only in recent weeks and have not yet been checked.

2 Three Sample Interferometers

We tabulate below important parameters for three sample interferometers, spanning a wide range of performance. The "Conservative" design relies almost exclusively on techniques and apparatus that have already been demonstrated in prototype research, and would be implemented only if no progress were made between now and the Design Freeze. The "Target" interferometer assumes steady progress in both experimental work and detailed design, and represents our estimate of reasonable parameters for Phase A interferometers. The "Advanced" detectors represents a critical look at the ultimate performance as limited by known sources of noise.

Parameters for 3 Sample Interferometers VER. 3.2			
Parameter	Conservative	Target	Advanced
——SHOT NOISE——			
Available Laser Power	5W	5W	100W
Heating Limited Loss/Mirror	0.2W	Not limited	Not Limited
Cavity Mirror Coating Loss	50 ppm	30 ppm	15 ppm
Injection Optics Loss/Comp.	V-coated	100 ppm	15 ppm
Photodetector Efficiency	0.8	0.8	0.8
Recycling	No	BB ×30	BB or RR ×100
Storage Time Corner Freq.	n.a.	7 Hz	11 Hz
——THERMAL NOISE——			
Dominant Loss Mechanism	?	?	Gas Damping
Suspended Mass	10 kg	10 kg	1 ton
Mechanical Q	10^7	10^9	10^{12}
——SEISMIC NOISE——			
Input Noise Spectrum	$10^{-7}\mathrm{m}\left(\frac{\mathrm{Hz}}{\mathrm{f}}\right)^2\mathrm{Hz}^{-1/2};\ (f > 10\mathrm{Hz})$		
Intra-vacuum Isolation	x:	$[2\ \mathrm{Hz} \times 5] \times [1\ \mathrm{Hz} \times 1]$	
	y:	$[7\ \mathrm{Hz} \times 5] \times [6\ \mathrm{Hz} \times 1]$	
Extra-Vacuum Isolation	None	$[1\mathrm{Hz} \times 1]$	

The tabulated choices for the shot noise parameters are based on the following considerations:

Available Laser Power The conservative and target designs assume

Argon lasers, as used in the prototype, one per interferometer. Two or more such lasers may be ganged together, but we do not analyze this arrangement. The entry 100 W for advanced designs assumes the availability of high-efficiency solid-state lasers. In all cases we assume the wavelength is 0.5 microns.

Mirror Heating The mirror-heating-limited power of 0.2 W per interferometer cavity mirror (0.8 W total loss distributed among 4 mirrors) is based on preliminary measurements of non-optimized mirrors. The "Not Limited" entry for target interferometers assumes reasonable progress from the mirror development program just getting underway.

Cavity Mirror Coating Loss The mirrors used in the Caltech prototype have approximately 50 ppm coating loss. The polishing and coating techniques are the same for ligo-sized mirrors, and we expect that the same quality of coating is obtainable. The achievement of 30 ppm loss coatings may be expected as a consequence of the mirror development program, and the measurement of loss as low as 15 ppm (for 0.63 micron light) has been reported in the literature.

Injection Optics Loss Anti-reflective coatings on the components between the laser and the beamsplitter determine the optical efficiency of the beam conditioning line. V-coatings are available from many manufacturers; 100 ppm A.R. coatings have been achieved by Litton; 15 ppm will require advances in coating technology.

Storage Time and Recycling The choice of cavity storage time (specified by a corner frequency) depends on the mirror losses; it sets the number of times the light can be recycled. See Section 4.1 below for the relation between loss, storage time, and recycling factor. In principle the storage time would be optimized relative to noise other than shot noise: a longer storage time reduces the shot noise at low frequencies at the expense of increased shot noise at high frequencies. In practice, there may be limitations other than mirror loss—such as the degree of phase front matching achievable with compensation plates—that limit the maximum number of recycles, consequently setting the

storage time. Lacking measurements, we have guessed broadband and resonant (BB and RR) recycling factors of 30 and 100 for the Target and Advanced receivers, respectively.

See below for an explanation of the parameters chosen for thermal noise and seismic noise.

3 Performance of Sample Interferometers

The graphs on the next three pages are experimentalists' curves for the expected performance of the three sample interferometers. They differ from previous curves (as presented, for example, in the December, 1987 proposal) in several respects:

- Seismic and thermal noise are explicitly calculated.
- The ordinate is amplitude spectral density of strain sensitivity, $h(f) = 2x(f)/L$, where $x(f)$ is the amplitude spectral density for motion of one of the four test masses. The conversion to sensitivity for periodic signals after measurement time $\hat{\tau}$ is given by $h_{\text{periodic}} = h(f)/\sqrt{\hat{\tau}}$. The conversion to sensitivity for burst signals depends on the burst waveform, but is given approximately by $h_{\text{burst}} = h(f)\sqrt{f}$.
- Each curve represents a single detector with the parameters indicated, not a family of optimized detectors.
- The strength of sources is not shown. The degradation of effective sensitivity due to poor statistics likely in the first searches (only a few events per month, say) is not indicated. The plotted curves correspond to unity signal-to-noise ratio.

3.1 Conservative Interferometer

The Conservative Interferometer we consider is a straightforward scaling up of the Caltech prototype, but with the addition of recombination and improved optical efficiency. It assumes no advances in mirror coatings or

substrate quality. Note though that the mechanical noise terms of the Conservative assumptions represent substantially better performance at low frequency than any of our prototypes have achieved to date, even taking account of length scaling. The plotted curves represent the best performance achievable, given these assumptions.

3.2 Target Interferometer

The Target Interferometer is what we have in mind for Phase A operations. It efficiently uses most of the 5 Watts available from a single laser in a broad-band recycling configuration. A detailed description of the optics and servos for this configuration is appended to the end of this report.

3.3 Advanced Interferometer

In addition to the photon shot noise, thermal noise, and seismic noise, the Advanced Interferometer graph shows a line labeled "Radiation Pressure Fluctuation." This effect grows with power, and becomes significant for the very high recycled power in this model. The crossing point between the radiation pressure and shot noise lines is the frequency where the sensitivity is set by the uncertainty principle (Standard Quantum Limit). Below this crossing frequency, the noise can be reduced to the quantum limit line by the simple expedient of lowering the power injected into the interferometer (at the expense of increased noise at higher frequencies).

4 Calculation of Noise

4.1 Shot Noise

For a recycled system with inner-cavity storage time corresponding to corner frequency f_k and with recycling factor b the shot noise sensitivity is

$$h(f) = \left(\frac{4\pi\hbar\nu}{\eta P b}\right)^{1/2} \frac{f_k}{2\nu}\sqrt{1+\left(\frac{f}{f_k}\right)^2}$$

where P is the power available (in the absence of recycling) at the photodetector having quantum efficiency η and ν is the optical frequency ($5.8 \cdot 10^{14}$

Hz). For the unrecycled case, $b = 1$. The maximum number of recycles is set by the sum of the losses in the two mirrors, L_m and the cavity length L:

$$b = \frac{2\pi L f_k}{c L_m}$$

where $c/2L$ is the free spectral range of the cavity (37 kHz for 4 km arms).

4.2 Thermal Noise

Thermal noise is the analog of Brownian motion for the test masses in the interferometer. Its existence is required by the fluctuation-dissipation theorem (Callen 1951,1952), which gives the fixed proportionality between a dissipative force (friction) and the resulting fluctuating force in any physical system. Thus the magnitude of the thermal noise depends on the size of the mechanical losses in the pendulum suspension.

Pendulum suspensions are chosen because they are known to exhibit low losses. Some of the loss mechanisms, especially external ones such as friction from residual gas, are straightforward to calculate. Other loss mechanisms are due to phenomena occurring in the flexing members which hold up the test mass. The spectrum of these mechanisms exhibits all of the richness of solid state physics. The magnitude of these effects is the subject of ongoing research. At present we can only estimate the likely values.

In the absence of a complete model of suspension losses, we have chosen to represent the thermal noise with a white noise spectrum, parametrized by the dimensionless number Q. (The white spectrum is a good representation of viscous damping, as well as of material damping mechanisms characterized by relaxation times short compared to the inverse of the highest frequencies of interest to us. Mechanisms with longer relaxation times generate forces with spectral densities which fall with increasing frequency.)

When the losses do give a white spectrum, its magnitude is

$$F^2(f) = \frac{8\pi k T m f_0}{Q}.$$

Here, m is the mass and f_0 is the resonant frequency of the pendulum.

Our three models for interferometer thermal noise were chosen as follows. We assumed a resonant frequency of the final pendulum stage as 1

Hz for all models. The Conservative and Target models assumed a mass of 10 kg, the natural size for a mirror for a Fabry-Perot interferometer for a 4 km arm length. The Advanced model uses a mass of 1 ton, both to lower the thermal noise and to minimize quantum noise.

The Conservative model assumes a $Q=10^7$, a value which has been measured in carefully constructed pendulums. For the Target model, we assumed that with better understanding of the loss mechanisms we could achieve a $Q=10^9$. Finally, we took a value of $Q=10^{12}$ for the Advanced model. None of these values is inconsistent with the loss mechanisms which we do understand.

The vertical thermal noise motion of the test masses may dominate the horizontal thermal noise discussed here, especially with anisotropic suspensions of the type considered so far. The vertical mode of a pendulum is typically substantially lossier than the horizontal mode. If its Q is poorer by more than about a factor of 10^5, then the vertical noise may dominate the thermal noise spectrum. This is unlikely to be important in the Conservative or Target systems, but may lead to poorer performance than we have predicted for the Advanced model.

4.3 Seismic Noise

The test masses of the interferometer must be shielded from the large ambient vibration spectrum of the terrestrial environment. We estimate the residual seismic noise by multiplying a typical ambient spectrum by the transfer function of the multi-stage vibration isolation system which supports each test mass.

The heart of the vibration isolation system consists of several passive stages located inside the vacuum system. The ultimate stage is the pendulum suspension of the test mass. It is supported in turn by a set of alternating masses and compliant elements called a "stack". The whole system functions as a low pass filter with many poles.

To first order, the interferometer is sensitive only to motions of the test masses along the optic axis. Typically, this is arranged to be horizontal, because pendulums are better horizontal isolators than they are vertical isolators. Also, the low-loss property of pendulums applies primarily to horizontal motions of the test mass. Finally, at all stages of the

vibration isolation system, it is usually somewhat easier to add compliance in the horizontal than in the vertical. Thus, isolation systems are rather anisotropic. Input spectra, on the other hand, are approximately isotropic.

If the optic axis departs from the horizontal, then the suspension anisotropies become important. This could come about if, for reasons of cost or convenience, the interferometer is installed along a slope. There is an unavoidable departure of the optic axis from the horizontal in a large interferometer, due to the curvature of the earth. At minimum, this amounts to the equivalent of a 0.3 mrad slope at each test mass. This means that if the vertical noise of the test mass is more than 3×10^3 times greater than the horizontal noise, then it will dominate.

For the model vibration isolation systems which are part of the designs presented here, we considered a range of slopes for the interferometer arms, from 0.3 mrad (the effective slope of an ideally prepared site) to 3 mrad (the specification in the Design Handbook). Even for an ideal site, the vertical noise is much more important than the horizontal noise. This suggests that we should apply extra effort to the design of isolators which work well in the vertical direction.

For the Conservative model, we assumed that the pendulum had a 1 Hz resonance in the horizontal, 6 Hz in the vertical. The stack has five layers, each characterized by a 2 Hz resonance in the horizontal, and a 7 Hz vertical resonance.

The Target model adds to this isolation system an isotropic 1 Hz isolator, assumed to be a feedback-controlled air spring mounted externally to the vacuum chamber. We used the manufacturer's data[1], which show a 2-pole roll-off between 1 Hz and 30 Hz, in estimating the effectiveness of this stage.

We planned to include the use of the suspension point interferometer in the Target model. However, the performance of such a system is poor in situations where the vertical noise dominates the horizontal noise. Therefore, until we design a passive isolation system in which the horizontal noise is the dominant factor, we can not count on noise reduction from the suspension point interferometer.

We did not specify the isolation system for Advanced detectors, beyond

[1] *The Newport Catalog*, No. 100, p. A–25.

using the specifications for the Target model. We note that, even with the dominance of vertical noise in the Target system, seismic noise dominates the already good thermal noise level in the Target interferometer only below 15 Hz. It dominates the spectrum of the Advanced detector also only below 15 Hz; at higher frequencies, quantum noise is larger than seismic noise.

5 Conclusions and Work in Progress

We emphasize the preliminary nature of this work, and release this version to stimulate comments.

The three sample interferometers were chosen to indicate a range of sensitivities that may be achieved in ligo. The Target specification is our best guess for the first receiver, but there remains considerable uncertainty as to its performance, especially in the significant band dominated by thermal noise. We have omitted consideration of techniques to go beyond the standard quantum limit; the one proposal we know of is for narrow-band searches only. The sensitivity improvement to be obtained from squeezed light techniques has not been analyzed.

Possibilities for additional work include:

- An analysis of resonant and double recycling, including comparison of the results with published work.
- If the vertical motion can be reduced by increasing the vertical compliance of the stacks over what we have assumed here or by adding springs, the suspension point interferometer becomes valuable for low frequency operation. Other enhancements which have been suggested but not yet fully analyzed are anti-seismic reference arms and vertical interferometers between the suspension points and test masses.
- Additional calculations and measurements of thermal noise.
- A detailed analysis of the conditioning optics, including specifications on components such as power handling capability, wave front distortion and clear aperture.

- An analysis of the main interferometer frequency stabilizing servos, including interaction of loops during lock acquisition and normal operation.
- An analysis of pointing accuracy requirements, and pointing servo performance.

Figure Caption—Broadband Recycling

Optical Layout: Light from the laser is prestabilized by locking to a small reference cavity (not shown). Approximately 90% of the laser output power passes through the input mode cleaner **MC1**, which provides a wavelength reference for further servo-driven reduction of frequency noise in the signal band, reduces geometric fluctuations in the beam, and attenuates out-of-band (> 1 MHz) noise. After being split at beam splitter **B**, the light is injected into the 4 km cavities, implemented by applying high quality reflective coatings on the faces of test masses **TM1**, **TM2** and **TM3**, **TM4**. The light coming back from these cavities is recombined at **B** and analyzed by the photodiodes **D5** (antisymmetric output) and by **D6** and **D7**. The interferometer is operated on a dark fringe at the antisymmetric output, so that practically all the light comes out of the symmetric output. The recycling mirror **rm** sends the light back into the interferometer, thus increasing the actual circulating power and reducing the photon shot noise. The output mode cleaner **MC2** attenuates geometric fluctuations in the output beam and scattered light reaching the main photodiode **D5**. The filter cavity **FC** extracts the light needed for keeping the beam splitter in the right place, as explained below. **PO1,2** are pick-off plates that divert a small fraction of the light ($\sim 1\%$) to Pockels cells **PC3,4**, where phase modulation is applied to the beams (side arm modulation technique) and to **D6,7**. **PO2** also compensates for the additional optical path in the horizontal arm, due to the thickness of the beam splitter.

Servo Controls: Several servo systems are needed for keeping the various cavities in resonance with the light. The technique generally used has been described elsewhere *(to be written as a part of the proposal).* The optical circulators required for the locking consist either of a polarizing beam splitter (**B1, B3, B4**), and a quarter wave plate (**wp**) or of a polarizing beam splitter and a Faraday rotator (**B2, fr**).

- The main mode cleaner **MC1** is locked by using modulation frequency f_1, applied to **PC1**. The error signal is derived from photodiode **D1**. The length of **MC1** is chosen to pass the f_1 sidebands (e.g. 12.5 m for $f_1 = 12$ MHz).

- The resonator consisting of the recycling mirror and the rest of the interferometer is locked by using the modulation f_1. The error signal is derived from photodiode **D2**.

- The Michelson interferometer consisting of the main beam splitter **B** and the input mirrors **TM1** and **TM3** is locked on a dark fringe by using light at an offset frequency. This is done by applying to **PC2** a very high frequency subcarrier f_4 ($\sim$ 500 MHz) that is phase modulated at f_3. After interacting with the side arm Pockels cells **PC3,4**, the subcarriers also carry phase modulation at $f_{1,2}$. At the antisymmetric interferometer output, only sidebands corresponding to f_1 (which is applied in antiphase to the sidearms) and f_3 are present. The f_3 signal at **D4** is used to lock filter cavity **FC** to one of the subcarriers. **FC** rejects the other subcarrier and the carrier (which contains most of the incident light), but transmits the sidebands corresponding to f_1. The f_1 signal at **D3** is used to maintain a dark fringe by adjusting the beam splitter position.

- The output mode cleaner **MC2** is locked to the carrier by using the f_4 signal at **D4**. The length of this mode cleaner is chosen to pass the f_1 sidebands.

- For the interferometer to function, both 4 km cavities have to be kept in resonance. The error signal is derived symmetrically, by summing the f_2 pieces of the sidearm signals from **D6** and **D7**. Deviation from resonance due to residual laser frequency fluctuations is common to both cavities, and the correction signal is applied both to the vertex station test masses (**TM1,3**), and to the side arm Pockels cells **PC3,4**.

- The gravity-wave signal is detected by **D5**, which looks at the antisymmetric interferometer port. This signal is used to adjust the length of one of the cavities (by pushing **TM4**), so that the interferometer is kept on a dark fringe to high accuracy. The gain of this loop is high at gravity-wave frequencies, and the ultimate gravity-wave signal is the feedback voltage applied to **TM4**. The signal at **D5** is contaminated by noise due to the low light level in the beam splitter

control loop (only part of the subcarrier at f_4 is used). After double integration to compensate for the mechanical transfer function of the beam splitter, this noise is subtracted from the **D5** signal before being fed back.

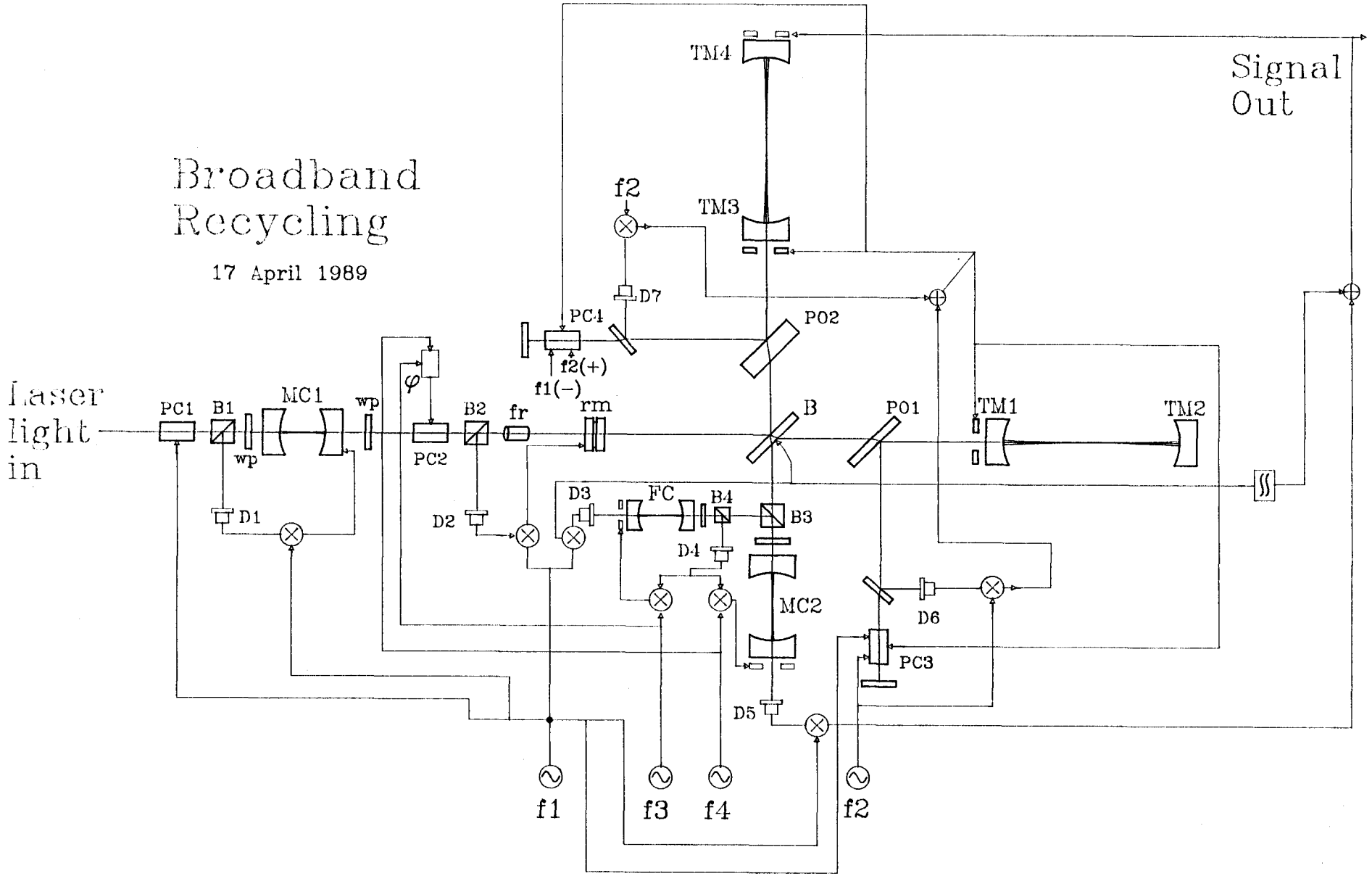
Broadband
Recycling
17 April 1989
Laser
light
in
Signal
Out
TM4
TM3
TM2
TM1
f2
D7
PC4
f2(+)
f1(−)
PO2
PO1
B
PC1
B1
wp
MC1
wp
φ
PC2
B2
fr
rm
D1
D2
D3
FC
B4
B3
D4
MC2
D6
PC3
D5
f1
f3
f4
f2

CONSERVATIVE .

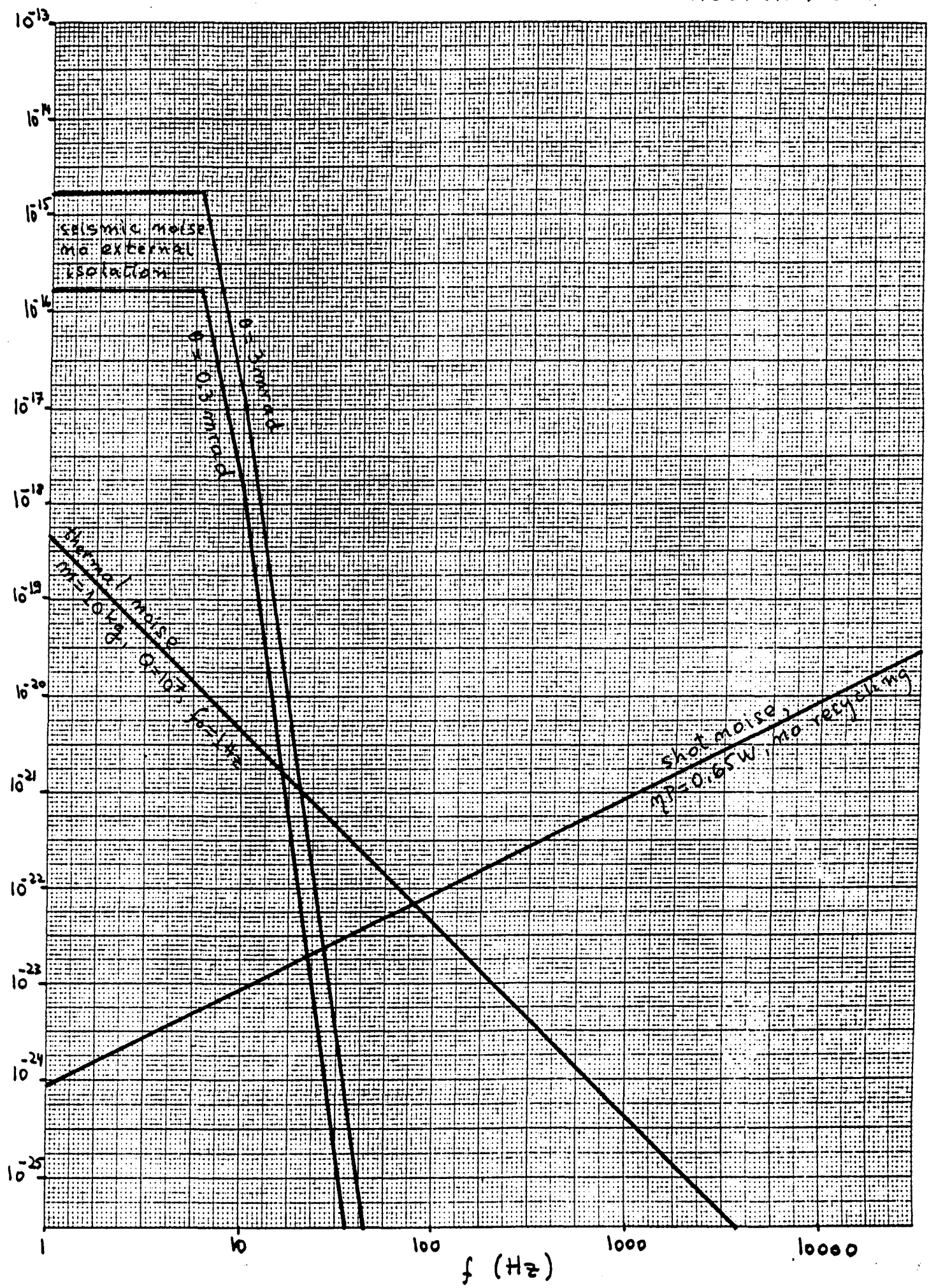

TARGET

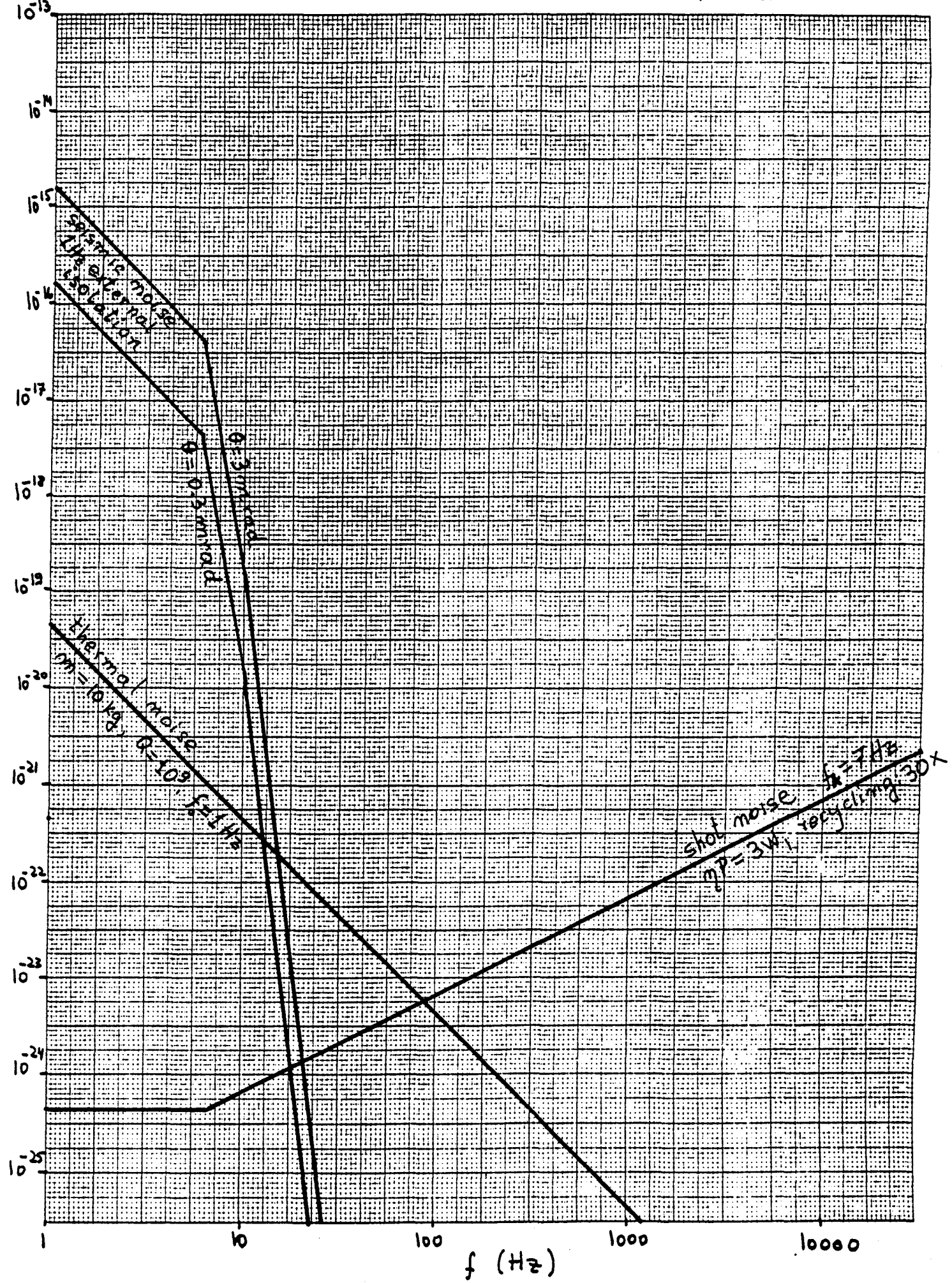

ADVANCED

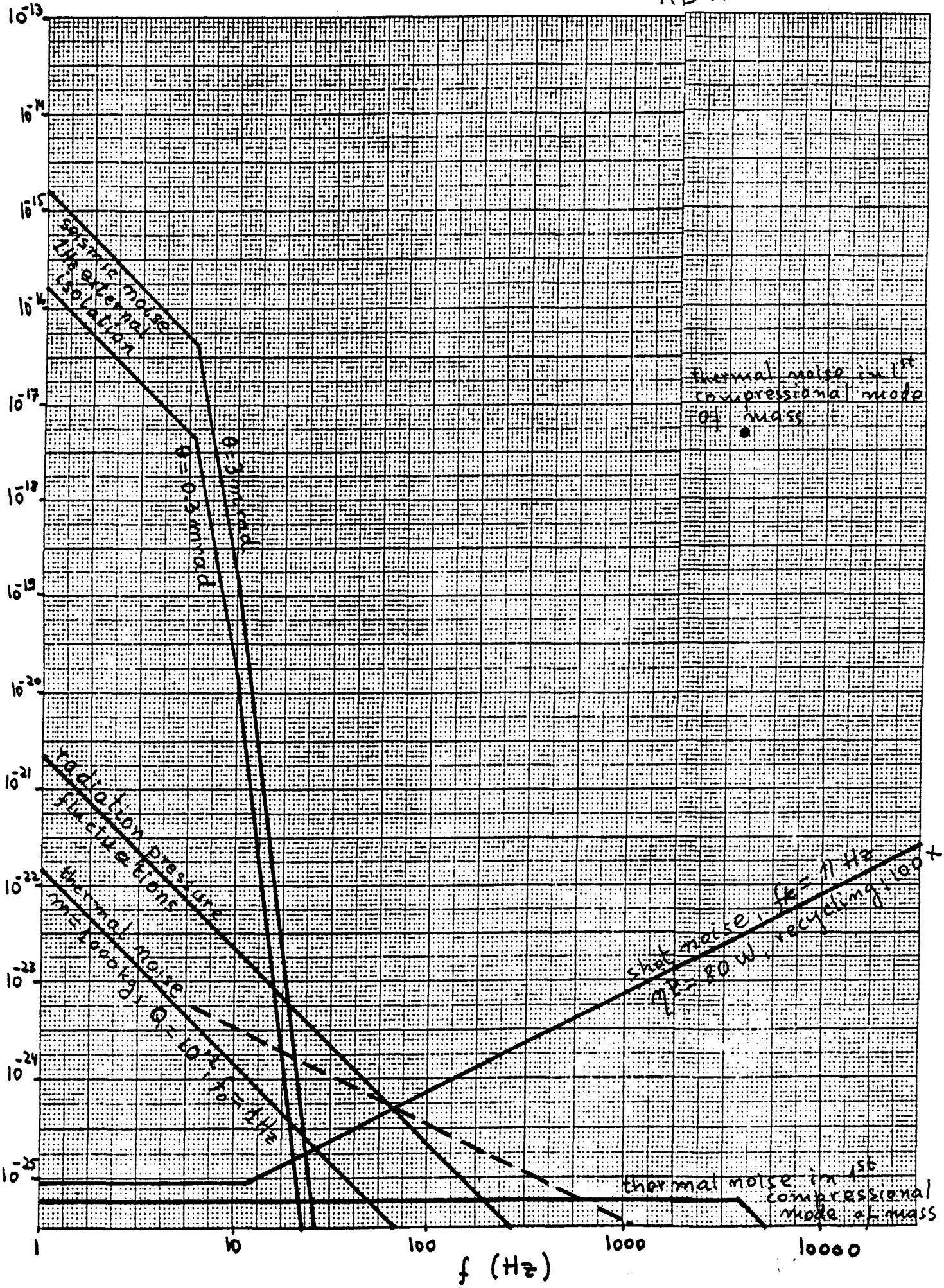

BATCH START

STAPLE
OR
DIVIDER

REPORT ON LIGO INTERFEROMETERS

2. Comments and Additions to the Report "Initial Design and Performance for Three Sample Configurations"

Ronald Drever (4-26-89).

1. Introduction.

The report on LIGO Interferometers "Initial Design and Performance for Three Sample Configurations", by A. Abramovici, P. Saulson and R. Spero (1) summarizes results of analyses of some factors limiting sensitivity in three versions of a family of gravity-wave receiver designs (2) which I developed mostly in summer 1987. It may help make some parts of the design of these interferometers clearer if I comment on aspects of the report (1) here, and add notes on some features devised since the original design was conceived, or not shown explicitly in the original report describing it.

2. Sample Interferometers Considered.

The optical design analyzed in (1) is in essence the same as the original, but is based on a more recent slightly modified drawing showing a symmetrical version of the modulation system. This was considered initially, but was not drawn then since it involved more optical components. However with a symmetrical system it is easier to see how excess noise from the low-power interferometer controlling the beamsplitter can be balanced out by electronic compensation, not shown explicitly before, and the symmetry gives convenient cancellation of some modulation sidebands (3).

The particular sample interferometers analyzed in the report (1) do not precisely match the original models. In part the differences have come from the fact that only initial analysis of the seismic isolation systems has been done so far, and the active anti-seismic systems have not been included. There has been some inaccuracy in the seismic noise estimates, and we will discuss this below.

The original design family includes a low frequency detector design. This is intended as a phase A design, but it would not be the first interferometer in the system, and it is not covered in the report (1).

(3) Notes on Seismic Noise.

The report (1) correctly points out the importance of vertical seismic isolation, and the difficulty of making passive vertical isolation as good as horizontal isolation. However it should be recognized that in high-attenuation seismic stacks the penetration of seismic noise is likely to be dominated by second order phenomena of various kinds, and particularly by cross coupling of vertical and horizontal motions, and not correspond only to the feedthrough predicted by simple 1-dimensional analyses. In the current rubber-steel stack design the relatively large horizontal attenuation expected from a simple model is likely to be seriously degraded by leakage from vertical motion. Experiments with the Pisa isolation system showed that cross-feedthrough of this type was near the same order of magnitude as direct feedthrough and a cross-coupling of similar order does not seem unlikely for the present system. If this is so it could lead to the following effects:-

(a) Seismic motion of the test masses will be more nearly isotopic than simple analysis would suggest.

(b) The relative degrading of horizontal isolation relative to vertical will make the overall isolation of passive stacks significantly poorer than shown in the curves given in the report.

(c) The reduction of vertical motion relative to horizontal at the test masses will make the proposed seismic monitor interferometer more effective than predicted, even in the presence of some ground slope. It might be expected that curves like those shown in the report would be more likely to be achieved with a seismic monitor interferometer than without it.

A full theoretical analysis of phenomena such as these may be difficult. Further experimental measurements may be useful.

References.

(1). "Report on LIGO Interferometers - Initial Design and Performance for Three Sample Configurations", by A. Abramovici, P. Saulson and R. Spero. (4-18-89)

(2). "Outline of a Proposed Design for a First Receiver for Installation in the Long-Baseline Facilities, of Fabry-Perot Type", by R.W.P. Drever (Internal Report, September 1987,

reissued as LIGO Report number 72).

(3). See, for example, the analysis by R. Weiss. (LIGO Report number 66. (3-14-89))